# Hydrogen-induced phase separation in amorphous $Cu_{0.5}Ti_{0.5}$ alloys. III. Computer-simulation studies

Bernard Rodmacq, Luc Billard, and Frédéric Lançon
*Groupe de Métallurgie Physique, Service de Physique, Département de Recherche Fondamentale, Centre d'Etudes Nucléaires de Grenoble, 85X-38041 Grenoble Cedex, France*
(Received 18 July 1988)

Neutron-diffraction results on amorphous CuTi hydrides have been used to construct a model for the structure of the amorphous matrix and the location of hydrogen. The important modification of the metallic matrix upon hydrogen absorption is simulated by a Monte Carlo procedure with nearest-neighbor exchanges on an $A_{50}B_{50}$ alloy with no size effect. Both initial (chemically ordered) and final (phase-separated) configurations are then numerically relaxed with a set of three Morse potentials in order to account for the size difference between Cu and Ti atoms. The influence of order and size difference on the distribution of interstitial sites is also studied. A good agreement with the experimental interference functions and reduced atomic distribution functions is obtained both before and after hydrogen loading. On the basis of the experimental results, hydrogen is then introduced in the metallic matrix by considering the occupancy of $Ti_4$ sites only and with hydrogen-hydrogen nearest-neighbor exclusion. Both the variation of the maximum hydrogen content with alloy composition and the partial metal-hydrogen and hydrogen-hydrogen atomic distribution functions are found to agree with experiment.

## I. INTRODUCTION

Whereas the first two papers of this series[1,2] were mainly devoted to the experimental study of the structure of amorphous CuTi hydrides, the present one is primarily concerned with the use of these experimental results as a starting point for computer-simulation experiments. The aim of this paper is first to analyze the structure of a computer model for amorphous alloys, with a particular attention to effects such as chemical order and size difference on the nature and number of interstitial sites, and second to apply this model to the case of hydrogenated copper-titanium amorphous alloys, looking at both the structure of the metallic matrix and location of the hydrogen atoms.

Concerning the hydrogen-storage properties of early-transition-metal–late-transition-metal (ETM-LTM) amorphous alloys, all the experimental results published up to now have pointed out that hydrogen preferentially occupies tetrahedral $B_4$ sites ($B$=Ti,Zr) in $AB$ alloys ($A$=Ni,Cu,Pd,Rh,Fe), and possibly $AB_3$ and $A_2B_2$ sites when the hydrogen concentration is increased. Although the preferential occupancy of given sites seems to be well established from neutron-diffraction measurements in Cu-Ti (Ref. 3) and Ni-Zr (Ref. 4) glasses through the observation of Ti-H or Zr-H distances in the pair correlation functions, or in Pd-Zr and Rh-Zr (Ref. 5) glasses from the increase of only the Zr-Zr distances upon hydrogen absorption in x-ray measurements, the possibility for hydrogen to occupy less favorable sites such as $AB_3$ and $A_2B_2$ has not been clearly demonstrated, except maybe in the case of Ni-Zr hydrides on the basis of neutron-scattering[4] or electrochemical[6] measurements.

Once the possible interstitial sites have been identified, one has to determine their relative occupancies as a function of total hydrogen content and composition of the alloy. As far as the hydrogen absorption capacity is concerned, it appears that simple models based on a statistical distribution of the interstitial sites [$Zr_4$ and $NiZr_3$ sites in Ni-Zr (Ref. 4) or $Zr_4$ sites in Zr-based amorphous alloys[5]] give a reasonable agreement with the experimental observations, at least for Zr concentrations smaller than 50% to 60%. For larger Zr concentrations, such models seem to overestimate the number of possible sites. The only way to balance this effect is to consider some repulsion between hydrogen atoms at short distance, analogous to the one observed in crystalline hydrides.[7] The introduction of such a repulsive interaction (leading to a minimum H-H distance of about 2.1 Å in crystalline hydrides) drastically decreases the number of available sites, since one occupied site will typically lead to the exclusion of the four neighboring ones (if all the sites are considered irrespective of their chemical identity). This effect will only be important at high-$B$ content in $A$-$B$ alloys when only $B_4$ sites are considered, as observed experimentally.[4,5] The analysis of a computer-generated model for Ni-Zr glasses[8] also leads to the same conclusion that a good agreement between experimental and calculated hydrogen-absorption capacity can be obtained if some minimum H-H distance (corresponding approximately to the exclusion of nearest-neighbor sites) is introduced.

At this stage, one has to recall that the above calculations (statistical distribution of sites or analysis of a computer model) have been carried out by supposing that the amorphous alloy was chemically disordered and made of atoms of the same size. This is clearly an oversimplification since all the ETM-LTM amorphous al-

 

loys studied by means of diffraction seem to exhibit some tendency towards chemical ordering. On the other hand, the size effect in these alloys is not at all negligible, since the ratio of the atomic diameters ranges between 1.15 for Ti-Cu and 1.28 for Zr-Ni alloys. Both effects of chemical ordering and (to less extent) of size difference will modify the relative proportions of the different sites. The hydrogen-absorption capacity will thus be also very dependent on the degree of chemical order, as it was already very dependent on both the type of sites considered and the short-range H-H interactions.

The present paper will try to address these issues. Section II will give details on the computer-simulation procedure used to obtain models with different degrees of chemical order (segregated, disordered, or ordered alloys) and on the topological analysis of these models. After having briefly recalled the main experimental results obtained on the amorphous Cu-Ti-H system by means of diffraction (Sec. III), we will use the models in Sec. IV to simulate the structure of the metallic CuTi matrix before and after hydrogen loading. Section V will be devoted to the study of the hydrogenation sites in relation with the results of neutron diffraction. The general discussion of the results will be given in Sec. VI.

## II. CONSTRUCTION AND ANALYSIS OF THE COMPUTER MODEL

### A. Monoatomic glass

To obtain amorphous structures with desired degrees of chemical order, we have used the Monte Carlo method on the topological configuration of a monoatomic glass. This procedure is described in Sec. II B. The monoatomic glass has been built with the static relaxation method: The potential energy of particles interacting through a pair potential $\phi(r)$ is driven to a local minimum by moving all the particles and by changing the atomic density.[9,10] A random assembly of hard spheres in a cubic box has been the starting configuration, and periodic boundary conditions have been used. We have built one model with 2048 atoms and one with 16 384 atoms, the larger one being used to obtain pair correlation functions on distances up to about 12 times the mean interatomic distance, thus limiting the termination effects in the calculation of the interference functions. The smaller model was used to analyze the structure of the interstitial sites in alloys with different degrees of chemical order, because of the much smaller computational time. The potential $\phi(r)$ is the Morse potential

$$\phi(r)=\epsilon_0(e^{-2\alpha(r-r_0)}-2e^{-\alpha(r-r_0)})$$

truncated at a distance $r_t$ equal to $1.15r_0$. $\phi(r)$ is equal to a fifth-order polynomial between $r_t$ and a cutoff distance $r_c=1.5r_0$ (at which the interactions are set to zero) so that $\phi(r)$ and its first and second derivatives are continuous at $r_t$ and $r_c$. $\epsilon_0$ and $r_0$ are, respectively, the depth and the position of the minimum of the potential, and we choose $\alpha$ such that $\alpha r_0=6$.

From the relaxed model, one calculates the pair correlation function $\rho(r)$ (number of atoms per unit volume at the distance $r$), the reduced pair correlation function $g(r)=\rho(r)/\rho_0$ (where $\rho_0$ is the average atomic density) and the reduced atomic distribution function $G(r)=4\pi\rho_0 r[g(r)-1]$. The interference function $S(q)$ is related to $G(r)$ by a Fourier transform:

$$q[S(q)-1]=\int_0^\infty G(r)\sin(qr)dr\ .$$

The $G(r)$ and $S(q)$ functions are presented in Figs. 1 and 2 in units of $r_0$ and $1/r_0$, respectively. The nearest neighbors are determined up to the first minimum of $G(r)$ at $1.38r_0$, leading to a value of the coordination number $Z=13.6$. The analysis of the structure is realized by decomposing the amorphous structure into Voronoi polyhedra. Every polyhedron defines a volume around each atom, a given point in this volume being at a smaller distance from the atom than from any other. Each Voronoi polyhedron corner is at equal distance from four atoms which form a tetrahedral interstitial site. Such an analysis leads to a complete decomposition of the structure into tetrahedra.[10]

In the amorphous structure, a large distribution of the size and shape of the tetrahedral sites is likely to occur. Some of them will be more or less distorted, and in this case it is possible to introduce some metric constraint on the bond angles or bond lengths between atoms. Batalla *et al.*[8] used such sort of a constraint by eliminating sites with bond angles smaller than 30° or larger than 90°. One can also define a maximum nearest-neighbor distance $r_{max}$: Every bond larger than $r_{max}$ is suppressed and the neighboring interstitial sites (i.e., those sharing this edge) are grouped together around this edge to form a larger site.[10]

The disadvantage of such methods is that the choice of these geometrical constraints on the bond angles or bond lengths between atoms is quite arbitrary, as for example the definition of a maximum nearest-neighbor distance since, contrary to the case of the Johnson potential, the minimum after the first peak of the reduced pair correlation function $g(r)$ does not go to zero in the case of the

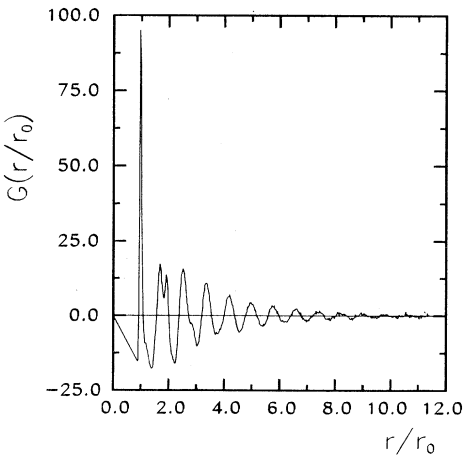


FIG. 1. Reduced atomic distribution function $G(r/r_0)$ for a monoatomic model of 16 384 atoms. $r_0$ is the position of the minimum of the Morse potential.

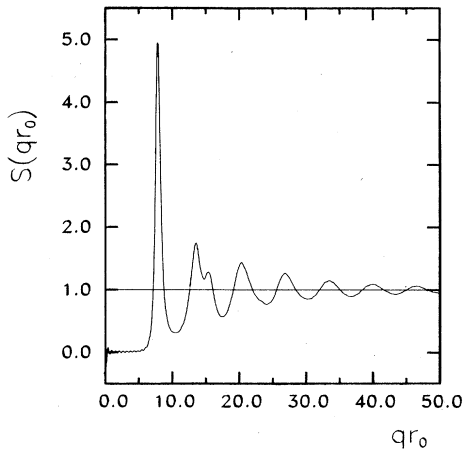


FIG. 2. Interference function $S(qr_0)$ for a monoatomic model of 16 384 atoms.

Morse or Lennard-Jones potentials.[10] In our case, we considered all the tetrahedral sites obtained by the decomposition of the structure into Voronoi polyhedra. We obtained a number of interstitial sites of 5.98 per metal atom.

### B. Chemical order and segregation

We will now study the influence of chemical order and segregation on $G(r)$, $S(q)$, and on the distribution of interstitial sites in a binary $A_{50}B_{50}$ alloy with atoms of the same size. This binary alloy is simply obtained by choosing $N_A$ and $N_B$ atoms ($N_A=N_B$) at random in the monoatomic relaxed model. The total pair correlation function is now the sum of three partial functions $\rho_{ij}(r)$ ($ij=AA$, $AB$, or $BB$) in the formalism of Faber and Ziman.[11] The partial coordination numbers $Z_{ij}$ are determined up to the first minimum $r_{\min}^{ij}$ of each function

$$G_{ij}(r)=4\pi r\left[\frac{\rho_{ij}(r)}{c_j}-\rho_0\right]$$

(the same one if no size effect) through

$$Z_{ij}=4\pi\int_0^{r_{\min}^{ij}} r^2\rho_{ij}(r)dr\ ,$$

and the short-range order parameter $\eta$ is calculated using the same definition as Spaepen and Cargill[12] except for the sign

$$\eta=1-\frac{Z_{AB}(c_AZ_A+c_BZ_B)}{c_BZ_AZ_B} \tag{1}$$

with $Z_A=Z_{AA}+Z_{AB}$ and $Z_B=Z_{BB}+Z_{BA}$. Finally, the analysis of the structure is carried out for the binary alloy in the same way as for the monoatomic case, except that there are now five types of tetrahedral sites $A_nB_{4-n}$ instead of one.

Since numerical relaxation with potentials of different depths cannot lead to chemical ordering or segregation (atoms cannot overcome energy barriers during the energy minimization, as would be required for a change in chemical order), one introduces chemical order or segregation by a Monte Carlo method: One $A$ and one $B$ atom chosen at random in the model are permuted with probability 1 if the possible resulting variation $\Delta_{BB}$ of the number of $B$-$B$ pairs is negative in case of order (or positive in case of segregation), and with probability $e^{-(|\Delta_{BB}|/T)}$ in the opposite case, the "temperature" $T$ being adjusted to give the desired value of the order parameter.

We will consider three cases: chemically ordered ($\eta=-0.10$), disordered ($\eta=0$), and segregated alloy ($\eta=+0.50$). In the formalism of Bhatia and Thornton,[13] the structure can be analyzed in terms of number-number, concentration-concentration, and number-concentration partial reduced atomic distribution functions $G_{NN}(r)$, $G_{CC}(r)$, and $G_{NC}(r)$ and partial interference functions $S_{NN}(q)$, $S_{CC}(q)$, and $S_{NC}(q)$.[14] In the absence of any size effect, the partial $G_{NC}(r)$ and $S_{NC}(q)$ functions are equal to 0, and the $G_{NN}(r)$ and $S_{NN}(q)$ functions are identical to the $G(r)$ and $S(q)$ functions of the monoatomic model (Figs. 1 and 2). Moreover $G_{CC}(r)=0$ and $S_{CC}(q)=c_Ac_B$ in the case of a chemically disordered alloy.

Figures 3(a) and 4(a) present the $G_{CC}(r/r_0)$ and $S_{CC}(qr_0)$ functions for the chemically ordered alloy and Figs. 3(b) and (4b) for the segregated alloy, respectively. For the ordered alloy, one observes a first negative peak in $G_{CC}(r/r_0)$ in Fig. 3(a) at the nearest-neighbor distance $r_1=0.97r_0$ (where $r_0$ is the position of the minimum of the potential), indicating preferred $A$-$B$ correlations. For the segregated alloy, the positive first peak in $G_{CC}(r/r_0)$ in Fig. 3(b) at the nearest-neighbor distance $r_1=0.97r_0$

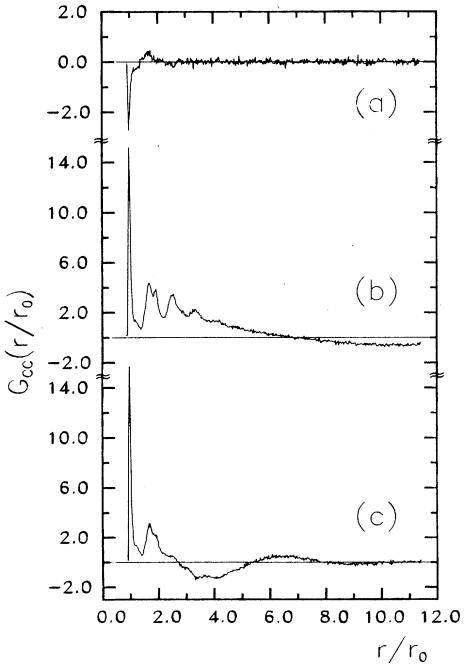


FIG. 3. Reduced atomic distribution function $G_{CC}(r/r_0)$ for (a) an ordered alloy ($\eta=-0.10$), (b) a macrosegregated alloy ($\eta=+0.50$), and (c) a microsegregated alloy ($\eta=+0.49$).

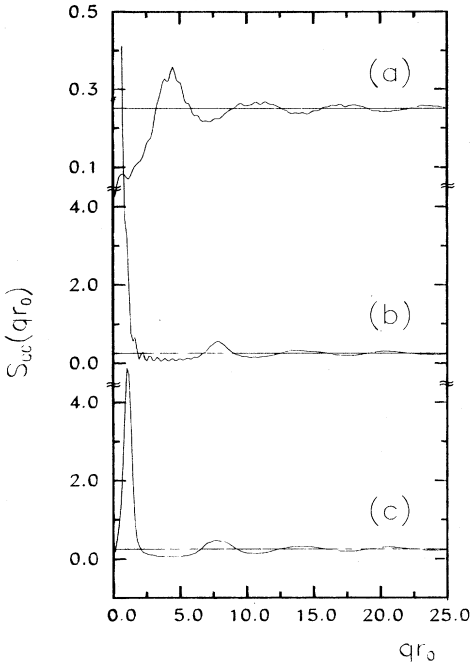


FIG. 4. Interference function $S_{CC}(qr_0)$ for (a) an ordered alloy, (b) a macrosegregated alloy, and (c) a microsegregated alloy.

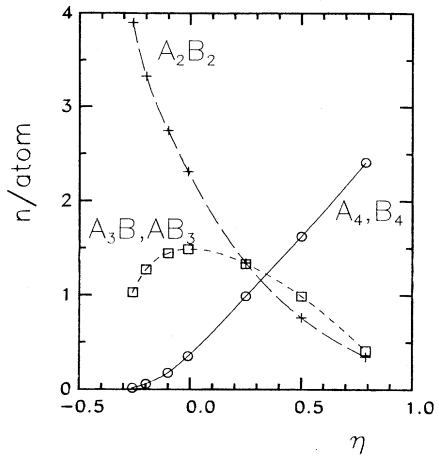


FIG. 5. Repartition of the number of $A_nB_{4-n}$ interstitial sites per metal atom in a $A_{50}B_{50}$ alloy as a function of the order parameter $\eta$.

indicates the presence of preferential $A$-$A$ and $B$-$B$ correlations. $G_{CC}(r/r_0)$ oscillates around an average value which decreases with increasing the distance, corresponding to a large distribution of the size of $A$ and $B$ clusters.

From these features one can simply predict the shape of the corresponding interference functions. Supposing that the $G(r/r_0)$ functions can be represented by a $\delta$ function, the Fourier transform of $G_{NN}(r/r_0)$ ($\delta$ peak at $r_1=0.97r_0$) will be a $(\sin qr_1/qr_1)$ function with a first maximum at $q_1r_1\simeq 7.72$, leading to $q_1r_0=7.72/0.97\simeq 7.9$, which compares well with the observed value of $q_1r_0=7.85$ in Fig. 2.

For the ordered alloy with a first negative peak in $G_{CC}(r/r_0)$ at $r_1=0.97r_0$, the first positive peak $q_Pr_0$ of $S_{CC}(qr_0)$ will correspond to the first *minimum* of $(\sin qr_1/qr_1)$, that is $q_Pr_1\simeq 4.49$, leading to $q_Pr_0=4.49/0.97\simeq 4.6$, to be compared to $q_Pr_0=4.52$ in Fig. 4(a). Moreover, $S_{CC}(qr_0)$ will oscillate out of phase with $S_{NN}(qr_0)$. For the segregated alloy with a first positive peak in $G_{CC}(r/r_0)$ at $r_1/r_0=0.97$, the corresponding $S_{CC}(qr_0)$ function will oscillate in phase with $S_{NN}(qr_0)$ with a first peak at $q_1r_0=7.9$, as observed in Fig. 4(b). In addition, the decreasing background in $G_{CC}(r/r_0)$ will lead to the appearance of a small-angle upswing in the interference function.

It is clear that the degree of order in these $AB$ alloys will modify the distribution of the interstitial sites $A_nB_{4-n}$. Figure 5 gives this distribution as a function of the order parameter $\eta$. The maximum segregation corresponds to $\eta_{\max}=+0.79$. $\eta_{\max}$ is smaller than 1 because of the limited total number $N$ of atoms in the model (for $c_A=c_B=0.5$, and supposing a complete separation between $A$ and $B$ atoms in the case of atoms of the same size, one would obtain $Z_{AB}=Z\times N^{-1/3}$ and $\eta=1-2\times Z_{AB}/Z=+0.84$ if $N=2048$ and 0.92 if $N=16\,384$). One can see in Fig. 5 that the number of $A_4$ and $B_4$ sites increases rapidly with increasing $\eta$. For an infinite model only these sites should be left for $\eta=+1$ (i.e., $Z_{AB}=0$). For the ordered alloy, the maximum order is obtained for $\eta_{\min}=-0.26$. The theoretical value of $\eta_{\min}=-(c_AZ_A/c_BZ_B)$ [cf. Eq. (1) with $Z_{AB}=Z_A$] corresponding to the case where $A$ ($B$) atoms are completely surrounded by $B$ ($A$) atoms can be only reached for $c_A$ ($c_B$) small because of frustration effects, contrary to the case of a $A_{50}B_{50}$ bcc structure, for example, where $A$ atoms occupy the vertices and $B$ atoms the center of the cube. Spaepen and Cargill[12] obtained a value of $\eta_{\min}=-0.27$ from the analysis of dense random packing (DRP) models at $c_A=0.5$. As a consequence of these frustration effects in the amorphous structure, one can see in Fig. 5 that the number of $A_3B$ and $AB_3$ sites does not vanish for the fully ordered alloy.

### C. Microsegregation

We will also consider another case of segregation which differs from the previously described procedure in two points: (1) We choose a null temperature, i.e., exchange is realized if and only if $\Delta_{BB}$ is positive or zero; (2) we restrict the permutations to $A$-$B$ nearest neighbors.

This case will be shown to apply to the amorphous CuTi hydrides (cf. Sec. III). Such a procedure is comparable to Monte Carlo simulations of first-order transitions with Kawasaki dynamics,[15] except that our calculations are carried out on an amorphous lattice at zero temperature. Under these conditions the system evolves towards a final state where atoms cluster together after a few nearest-neighbor exchanges. Since unfavorable permutations ($\Delta_{BB}<0$) are not allowed, this final state does not correspond to complete segregation between $A$ and $B$ atoms (i.e., $\eta=+1$) and the calculated short-range order

parameter is $\eta = +0.49$.

Figures 3(c) and 4(c) show the $G_{CC}(r/r_0)$ and $S_{CC}(qr_0)$ functions for this microsegregated alloy. Compared to the case of the macrosegregated alloy with the same $\eta$ [Fig. 3(b)], the short-range correlations extend now up to the second neighbors only. A long-period oscillation is also clearly visible in $G_{CC}(r/r_0)$ in Fig. 3(c) with its first maximum at $r_p \simeq 6.6 r_0$. The same reasoning as in the case of the macrosegregated alloy can be used here. Thus the interference function will present a peak at $q_1 r_0 = 7.9$ and will oscillate in phase with $S_{NN}(qr_0)$. In addition, the long-period oscillation in $G_{CC}(r/r_0)$ will correspond to the appearance of a small-angle peak at $q_0 r_0 = q_P r_P \times r_0 / r_P = 7.72/6.6 \simeq 1.17$, in agreement with the observed maximum in Fig. 4(c) at $q_P r_0 = 1.1$.

This process of microsegregation is likely to depend on the chemical order of the starting configuration, since an initially segregated state with $\eta = +1$ will obviously remain unchanged after such a process. Figure 6 gives the variation of the resulting order parameter $\eta_{\text{fin}}$ and position of the small-angle maximum $q_P r_0$ in $S_{CC}(qr_0)$ as a function of the initial order parameter $\eta_{\text{init}}$. One sees that, for $\eta_{\text{init}} \leq 0$, $\eta_{\text{fin}}$ and $q_P r_0$ are not very dependent of the initial chemical order. From the comparison between the macro- and microsegregated alloys, it appears that, although both alloys have the same order parameter, they differ strongly in terms of distribution of partial coordination numbers, as shown in Fig. 7 for the *B-B* distribution. The same average value (i.e., same $\eta$) is obtained but the distribution is much broader in the macrosegregated case. On the other hand, the analysis of the interstitial sites shows that the distribution in number of $A_n B_{4-n}$ $(0 \leq n \leq 4)$ sites is very similar for both samples.

Figure 8 compares the structure of the three alloys studied (ordered, macro-, and microsegregated) by showing a cut into the models. Contrary to the macrosegregated case where clusters of various sizes are present, only one characteristic length exists in the microsegregated alloy. Such a characteristic length corresponds to the

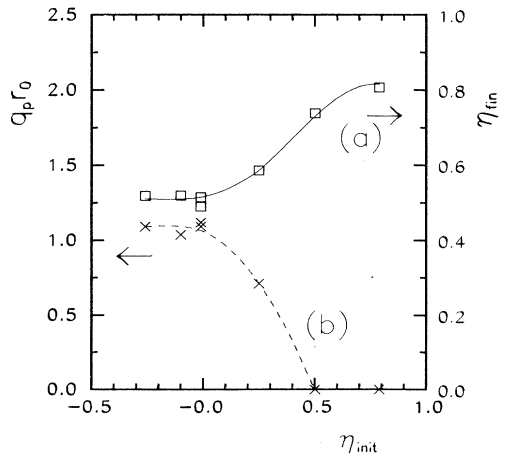


FIG. 6. Final order parameter (a) and position of the small-angle maximum (b) after the microsegregation procedure as a function of initial order parameter. The solid and dashed lines are guides to the eyes.

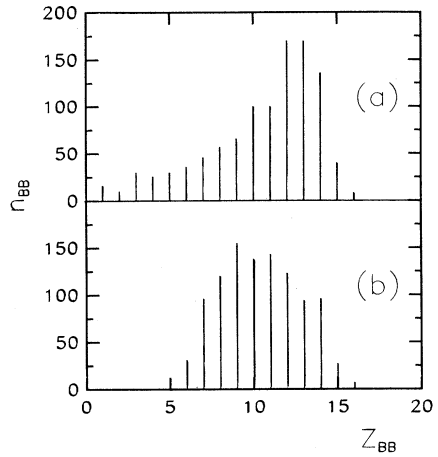


FIG. 7. Distribution of the *B-B* coordinance for two $A_{50}B_{50}$ alloys with same order parameter $\eta = +0.5$: macrosegregated (a) and microsegregated (b).

long-period oscillation in $G_{CC}(r/r_0)$ and to the small-angle maximum in $S_{CC}(qr_0)$ in Figs. 3(c) and 4(c).

### D. Size effect

Size effect has been studied by relaxing the binary models presented above with three Morse potentials of equal

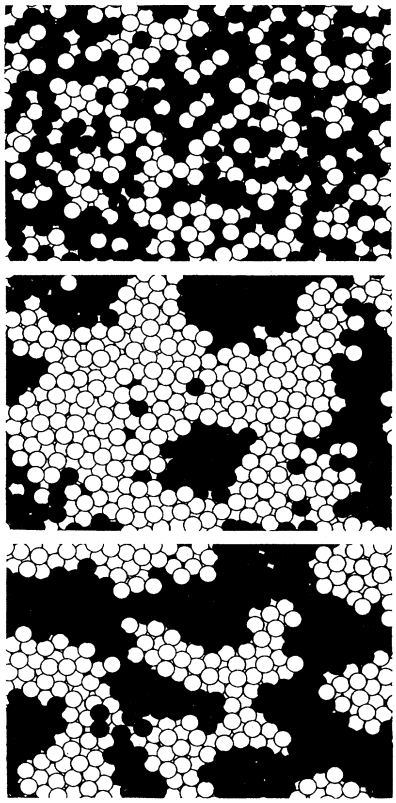

FIG. 8. Visualization of three models: ordered (top, order parameter $\eta = -0.1$), macrosegregated (center, $\eta = +0.5$), and microsegregated (bottom, $\eta = +0.5$).

depths in which the positions of the minimum are now different and equal to $r_{AA}$, $r_{AB}$, and $r_{BB}$ for the $AA$, $AB$, and $BB$ atomic pairs, respectively. We used the values of $r_{BB}/r_{AA}=1.14$ and $r_{AB}=(r_{AA}+r_{BB})/2$ (these values will be used in Sec. IV). The analysis of the interstitial sites was carried out using a Voronoi decomposition as described previously. For alloys of atoms of different sizes, the radical plane method[16] could also be used. In this case a volume in relation to the atomic radii is attributed to each atom, and one can expect a slightly different distribution of the interstitial $AB_3$, $A_2B_2$, and $A_3B$ sites as compared to the Voronoi method with essentially no modification of the number of $A_4$ and $B_4$ sites. As we will see in the following sections, we will only consider $Ti_4$ sites as possible sites for hydrogen occupancy. The Voronoi decomposition (with no adjustable parameter) was thus preferred over the decomposition into radical planes which depends on the atomic radii.

Starting from three different alloys of atoms of the same size (ordered alloy with $\eta=-0.10$, disordered alloy with $\eta=0.00$, and macrosegregated alloy with $\eta=+0.50$), Table I shows the influence of size difference ($r_{BB}/r_{AA}=1.14$) on the partial coordination numbers, resulting order parameter, and distribution of $A_nB_{4-n}$ sites. The variation of $\eta$ is induced by the size difference since the larger atom has on the average more neighbors than the smaller one. The distribution of sites is no longer symmetrical and now favors the sites made of the larger atoms ($A_4 \leq B_4$, $A_3B \leq AB_3$).

## III. EXPERIMENTAL RESULTS ON AMORPHOUS $Cu_{0.5}Ti_{0.5}$ ALLOYS AND HYDRIDES

Since the results of diffraction experiments have been given in details in a preceding paper,[1] we will just briefly recall them here and point out their implications for both the structure of the CuTi amorphous alloys and hydrides and the metal-hydrogen interactions.

As mentioned in the Introduction, the first neutron-diffraction experiments on CuTi glasses[17] showed that these alloys were chemically ordered, with a short-range order parameter $\eta$ of $-0.11$ to $-0.13$. It should be noted that this parameter $\eta$ was extracted from a combination of x-ray and neutron experiments and supposing no size difference between copper and titanium atoms. Our first computer-simulation studies[18] also showed that a good agreement between experimental and simulated neutron pair correlation functions could only be obtained through the introduction of some chemical order between Cu and Ti atoms (corresponding to $\eta=-0.10$).

Upon hydrogen absorption, the first experimental result is the appearance of Ti-H correlations in the total neutron pair correlation function whatever the hydrogen concentration,[1,3] thus indicating a preferential filling of $Ti_4$ tetrahedral sites by hydrogen atoms. At first sight this result seems quite surprising since the hydrogen-absorption capacity (maximum hydrogen content) in these $Cu_{0.5}Ti_{0.5}$ alloys amounts to about 0.7 to 0.8 (hydrogen per metal).[1,19,20] On the basis of a simple statistical distribution of sites with a mean number of tetrahedra per metal atom of about 6 (cf. Sec. II), the maximum number of $Ti_4$ sites would be $6\times0.5^4=0.37$ sites per metal atom for a chemically disordered alloy, and even smaller in the case of Cu-Ti alloys because of chemical ordering. Moreover, the effective number of occupied sites should be greatly reduced if some repulsive H-H interaction is considered.

Starting from the chemically ordered CuTi alloy, one way to increase the maximum hydrogen content is to consider a possible occupancy of other sites in addition to the $Ti_4$ ones ($Ti_3Cu$ and $Ti_2Cu_2$ for example), which seems to be experimentally excluded since it would lead to either the appearance of an intense Cu-H nearest-neighbor peak (if the Cu-H distance is different enough from the Ti-H one) or to an almost complete compensation of the Ti-H and Cu-H contributions (since the neutron-

TABLE I. Influence of size effect in a $A_{50}B_{50}$ alloy on the partial coordinances $Z_A$ and $Z_B$, order parameter $\eta$, and number of $A_nB_{4-n}$ ($n=0$–4) interstitial sites per atom for three alloys with different initial order parameters.

| | $r_{BB}/r_{AA}=1.00$ | | $r_{BB}/r_{AA}=1.14$ | | |
|---|---|---|---|---|---|
| $\eta_{init}$ | $Z_A,Z_B$ | $A_nB_{4-n}$, $n=0,1,\ldots,4$ | $Z_A,Z_B$ | $\eta$ | $A_nB_{4-n}$, $n=0,1,\ldots,4$ |
| $\eta=-0.10$ | 13.8,13.8 | 0.16 | 12.6,14.9 | $-0.07$ | 0.31 |
| | | 1.47 | | | 1.74 |
| | | 2.75 | | | 2.61 |
| | | 1.42 | | | 1.14 |
| | | 0.18 | | | 0.16 |
| $\eta=+0.00$ | 13.8,13.8 | 0.35 | 12.9,15.1 | $+0.00$ | 0.48 |
| | | 1.51 | | | 1.72 |
| | | 2.31 | | | 2.22 |
| | | 1.46 | | | 1.27 |
| | | 0.35 | | | 0.27 |
| $\eta=+0.50$ | 13.8,13.8 | 1.62 | 13.4,14.2 | $+0.44$ | 1.63 |
| | | 0.94 | | | 0.98 |
| | | 0.88 | | | 0.95 |
| | | 0.96 | | | 1.10 |
| | | 1.58 | | | 1.31 |

scattering length of copper is more than twice that of titanium and of opposite sign).

Another way is to modify the metallic matrix in some manner, i.e., to introduce some segregation between Cu and Ti atoms in order to increase the number of Ti-Ti pairs, and thus the number of $Ti_4$ sites. We already mentioned this possibility,[18] which has been recently confirmed by our neutron-scattering experiments with hydrogen-deuterium substitution on alloys with a hydrogen-to-metal ratio of 0.84.[1] Compared to the pair correlation function of the $Cu_{0.5}Ti_{0.5}$ alloy (with a tendency towards chemical order, i.e., more Cu-Ti pairs than for a disordered alloy), the function for the hydrogenated sample (in which the hydrogen-to-deuterium ratio leads to a negligibly small weight of the metal-hydrogen and hydrogen-hydrogen contributions) shows a quasiabsence of the Cu-Ti correlations, indicating that now a strong tendency towards segregation between Cu and Ti atoms exists in the hydrogen-loaded alloy. Moreover the corresponding interference function $S(q)$ shows the presence of a strong small-angle maximum at about 0.4 $\text{Å}^{-1}$. The position of this maximum and the variation of its intensity with hydrogen or deuterium loading indicate that such a segregation occurs between Cu and (Ti,H) regions on a very small scale of the order of 10 to 15 Å.

## IV. SIMULATION OF THE AMORPHOUS CuTi MATRIX

### A. Without hydrogen

Since as-quenched CuTi alloys exhibit a tendency towards chemical ordering, our starting point for modeling these glasses will be the monoatomic model of 16 384 atoms in which some chemical order has been introduced by a Monte Carlo procedure (Sec. II B), with an order parameter $\eta=-0.10$. From this model of atoms of the same size, the size difference between Cu and Ti atoms is now taken into account by carrying out the numerical relaxation with a set of three Morse potentials of equal depths, the position of the three minima being taken as the nearest-neighbor distances in pure crystalline Cu and Ti ($d_{\text{CuCu}}=2.55$ Å and $d_{\text{TiTi}}=2.91$ Å), and with $d_{\text{CuTi}}=(d_{\text{CuCu}}+d_{\text{TiTi}})/2=2.73$ Å. The three reduced atomic distribution functions $G_{\text{CuCu}}(r)$, $G_{\text{CuTi}}(r)$, and $G_{\text{TiTi}}(r)$ are then calculated from the positions of the atoms in the relaxed model. From the position of the minimum after the first peak of each $G_{ij}(r)$, partial coordination numbers of 5.3, 7.3, and 7.6 for Cu-Cu, Cu-Ti, and Ti-Ti pairs were calculated, leading to a value of the order parameter $\eta=-0.07$, to be compared to the initial value $\eta=-0.10$ in the alloy with no size effect (cf. Table I).

In order to compare experimental and simulated reduced atomic distribution functions and interference functions, the following procedure was used. Starting from the simulated $G_{ij}(r)$ functions, the partial interference functions $S_{ij}(q)$ were obtained by a Fourier transformation, the large cutoff value in direct space for the model of 16 384 atoms leading to negligible termination effects in $S(q)$. After that the total neutron-interference function was calculated through

$$S(q)-1=\sum_i \sum_j (c_i c_j b_i b_j/\langle b^2\rangle)[S_{ij}(q)-1] \tag{2}$$

with $\langle b^2\rangle=\sum_i c_i b_i^2$, $b_i$ being the neutron-scattering length of element $i$.

Since both calculated $G(r)$ and $S(q)$ functions correspond to a static state, it is necessary to account for thermal vibrations in order to compare them with the experimental functions obtained from room-temperature data. In a classical approximation the reduced pair correlation function $g_T(r)$ and interference functions $S_T(q)$ calculated at temperature $T$ are related to the static ones by the relations

$$S_T(q)-1=e^{-\sigma^2 q^2}[S(q)-1] \tag{3}$$

and

$$g_T(r)=\frac{1}{2\sigma r\sqrt{\pi}}\int u g(u) e^{-(r-u)^2/4\sigma^2}\,du$$

with $\sigma^2=\langle u^2\rangle/3$, $\langle u^2\rangle$ being the mean-square displacement of the atoms from the lattice positions (assuming a common value for all the alloy elements). The main effect of such a correction will be a damping of the oscillations of $S(q)$ at large $q$ and a broadening of the first peaks of $g(r)$. Besides, the experimental $g(r)$ functions are obtained by a Fourier transform of the interference functions. Since these interference functions are extracted from experiments extending over a limited $q$ range, the Fourier transform will introduce a supplementary broadening of the peaks of the $g(r)$ functions, in addition to the thermal one. It will also lead to the appearance of spurious oscillations with a period of $2\pi/q_{\max}$, where $q_{\max}$ is the upper limit of the integration in reciprocal space. For the sake of comparison between experimental and simulated curves, we will thus proceed as follows. Starting from the "static" atomic distribution function $G(r)$ one calculates the corresponding interference functions $S(q)$ by a Fourier transform. Then one introduces the thermal vibrations on $S(q)$ through Eq. (3) by adjusting the amplitude of the high-$q$ oscillations of the simulated curve to those of the experimental curve. Finally the corresponding atomic distribution function $G_T(r)$ is obtained by a Fourier transform of the above $S_T(q)$ function using a high-$q$ cutoff similar to the experimental one. The initial atomic distribution function $G(r)$ obtained directly from the relaxed model will be also presented in the following figures.

Figure 9 presents the experimental and simulated $S(q)$ curves in the case of neutron scattering. The amplitude of the oscillations of the simulated curve was adjusted using a "thermal" broadening $(\langle u^2\rangle)^{1/2}=0.14$ Å, representing about 5% of the mean-interatomic distance (this value will be kept the same throughout the rest of this paper). A good agreement is obtained between simulated and experimental interference functions, except at small scattering vector, where the first peak of the simulated curve is found at $q\simeq 1.6$ $\text{Å}^{-1}$ instead of 1.9 $\text{Å}^{-1}$ for the experimental one. One should notice here that this interference function is the combination of the three partial Cu-Cu, Cu-Ti, and Ti-Ti curves, with a negative sign

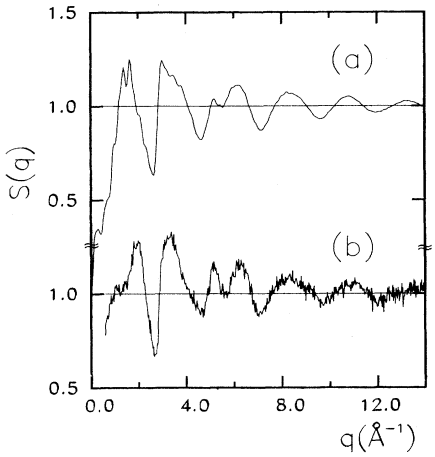


FIG. 9. Interference functions $S(q)$ for the initial $Cu_{50}Ti_{50}$ amorphous alloy: (a) simulated curve including the effects of thermal vibration and (b) experimental curve.

for the Cu-Ti one in the case of neutron scattering. According to that, the total $S(q)$ is dominated by the $S_{CC}(q)$ contribution, and it can be seen on Fig. 4(a), for example, that its amplitude is quite small compared with that of the $S_{NN}(q)$ contribution in Fig. 2 (this explains why termination oscillations are still visible on the simulated curve despite the large cutoff value in real space). Thus the position and intensity of any peak in this $q$ range will be very dependent on the exact shape of each partial $S_{ij}(q)$.

In Fig. 10 the overall shape and period of the oscillations of $G(r)$ are also well reproduced by the model

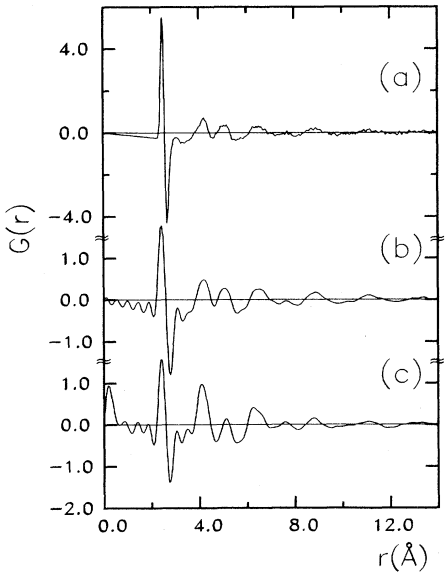


FIG. 10. Reduced atomic distribution functions $G(r)$ for the initial $Cu_{50}Ti_{50}$ amorphous alloy: obtained directly from the relaxed model (a), obtained from the Fourier transform of $S(q)$ in Fig. 9(a) with $q_{max}=13.9$ Å$^{-1}$ (b), and experimental (c). Note the different $y$ scale (a).

curve. Termination effects can be observed on the experimental curve in Fig. 10(c) on both sides of the main peak at about 2.5 Å, leading to the appearance of a supplementary small peak at about 3.5 Å, which can be also observed on the simulated curve in Fig. 10(b) obtained by a Fourier transform of $S(q)$. Another effect of the Fourier transform is to shift the first minimum of $G(r)$ from 2.7 to 2.8 Å. The agreement is also good at large distance, for both the position and intensity of the peaks up to 12 Å.

### B. With hydrogen

In the preceding section we recalled that the introduction of hydrogen in amorphous Cu-Ti alloys greatly changed the chemical order of the metallic matrix, leading to (i) a decrease of the contribution of the Cu-Ti pairs in the total reduced atomic distribution function and (ii) to the appearance of a small-angle maximum in the interference function. On the other hand, we showed in Sec. II C that the microsegregated model (in which the number of Cu-Ti pairs is decreased through local Cu-Ti permutations) led to $G(r)$ and $S(q)$ functions which met these requirements [cf. Figs. 3(c) and 4(c)]. We will thus simulate the structure of the metallic CuTi matrix after hydrogen loading by relaxing the microsegregated alloy obtained in Sec. II C with three Morse potentials, and using the same Cu-Cu, Cu-Ti, and Ti-Ti distances as in the case of the ordered alloy. In paper I we presented preliminary results of these simulations, the microsegregation being realized directly on the relaxed ordered model, with the disadvantage that such a procedure led to the formation of both high-density and low-density regions upon Cu-Ti exchanges. For the sake of simplicity, we have chosen here to separate ordering and relaxation procedures, the numerical relaxation being carried out on a topologically homogeneous alloy of atoms of the same size.

As we are now considering the hydrogenated CuTi alloy, the total reduced atomic distribution function $G(r)$ will be a linear combination of six partial functions $G_{ij}(r)$

$$G(r)=\sum_i\sum_j (c_i c_j b_i b_j)/\langle b^2\rangle G_{ij}(r) \quad i,j=\text{Cu, Ti, H} \ . \tag{4}$$

Since the (H,$D$) isotopic substitution allows one to change the neutron-scattering length of hydrogen, it will be possible to extract the metal-metal, metal-hydrogen, and hydrogen-hydrogen components from the total $G(r)$ through

$$\begin{aligned} G_{MM}(r)&=c_{\text{Cu}}^2 b_{\text{Cu}}^2 G_{\text{CuCu}}(r)+c^2 b_{\text{Ti}}^2 G_{\text{TiTi}}(r) \\ &\quad +2c_{\text{Cu}}c_{\text{Ti}}b_{\text{Cu}}b_{\text{Ti}}G_{\text{CuTi}}(r) \ , \\ G_{M\text{H}}(r)&=c_{\text{Cu}}b_{\text{Cu}}G_{\text{CuH}}(r)+c_{\text{Ti}}b_{\text{Ti}}G_{\text{TiH}}(r) \ , \\ G_{\text{HH}}(r)&=G_{\text{HH}}(r) \ . \end{aligned} \tag{5}$$

Let us note that $G_{MM}(r)$ and $G_{M\text{H}}(r)$ are characteristic of the metal-metal and metal-hydrogen correlations, respectively, but weighted by the scattering lengths of both metal atoms.

In the case where the mean scattering length of hydrogen is zero, the total $G(r)$ of Eq. (4) is directly proportional to $G_{MM}(r)$. As reported in paper I, one of our three neutron curves corresponds to a sample loaded with a mixture of hydrogen and deuterium, leading to a very small neutron-scattering length $b_{H,D}=-0.04\times10^{-12}$ cm compared with $b_{Ti}=-0.3438\times10^{-12}$ cm and $b_{Cu}=+0.7718\times10^{-12}$ cm and thus to a negligibly small contribution of the metal-hydrogen and hydrogen-hydrogen correlations in the total atomic distribution function and interference function. Figures 11 and 12 show the neutron $q[S(q)-1]$ and $G(r)$ curves for this sample along with the simulated ones. Since the factor $\langle b^2\rangle$ in Eq. (4) depends on the hydrogen concentration, we used the value determined in the next section in order to compute the simulated $G(r)$ curve. The overall shape of the experimental interference function is well reproduced by the simulated curve, although there is some discrepancy on the relative intensity of the peaks. Since obtaining the experimental interference function from the intensity curve is quite difficult in hydrogen-containing substances (and even more in the case of amorphous materials[1]), it is not meaningful to compare in details experimental and simulated curve amplitudes.

Both simulated and experimental curves show the existence of a large peak at small scattering vector $q$. The position of this peak at about 0.4 $Å^{-1}$ is well reproduced by the simulation, but its intensity is larger than the experimental one, although its width is smaller. This could be the result of a less homogeneous phase separation in the CuTi sample compared to the simulated alloy, resulting in some distribution in the characteristic length scale of this phase separation, and thus in a broadening of the small-angle maximum. It should also be noted that the intensity of the maximum is very dependent upon its position (i.e., on the extent of phase separation). For example, our preliminary simulation study[1] was performed by permuting Cu-Ti atoms when the variation of the number of Ti-Ti pairs was strictly positive (contrary to the present case where permutations with no increase were allowed). This led to a slightly smaller degree of phase separation (the small-angle maximum being located at 0.5 $Å^{-1}$ instead of 0.4 $Å^{-1}$) and to a large decrease of the intensity of this maximum (by a factor of about 3).

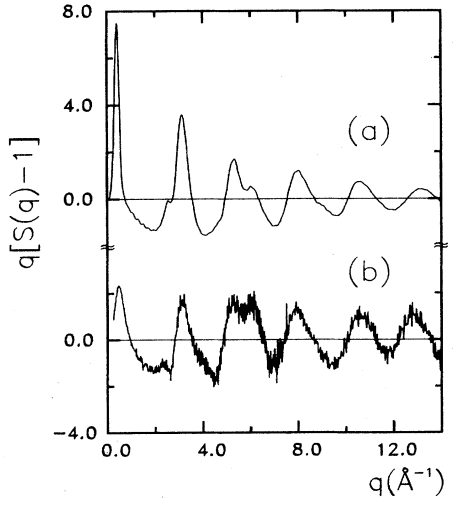


FIG. 11. Same as Fig. 9 for the CuTi matrix after hydrogen loading.

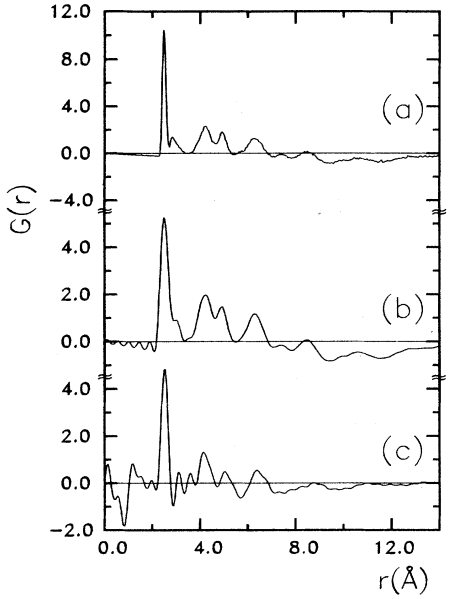


FIG. 12. Same as Fig. 10 for the CuTi matrix after hydrogen loading.

The same comments can be made when comparing the experimental and simulated $G(r)$ curves, with the additional problem of the Fourier transform of the experimental $S(q)$ which introduces oscillations on both sides of the main peak of $G(r)$. The long-period oscillation resulting from the phase separation is well marked in the $G(r)$ curves. Its amplitude is smaller in the experimental $G(r)$ [Fig. 12(c)] in connection to the smaller intensity of the small-angle maximum in $S(q)$. Nevertheless, these simulation results confirm the occurrence of a small-scale phase separation in amorphous CuTi alloys upon hydrogen absorption, and a satisfying agreement is obtained for both $G(r)$ and $S(q)$ curves on the basis of simple hypotheses and with a limited number of free parameters. We will now analyze the structure of the microsegregated model and introduce the hydrogen atoms in the interstitial sites following the procedure outlined in the preceding sections (preferential Ti-H correlations and short-range H-H repulsion) in order to account for the experimental hydrogen-to-metal ratio and to simulate the partial metal-hydrogen and hydrogen-hydrogen interference functions and atomic distribution functions.

## V. ANALYSIS OF THE HYDROGENATION SITES

Having proposed in the preceding section a model of the structure of the amorphous CuTi matrix after hydrogen loading, we will now analyze this model in order to identify the type and number of interstitial sites for hydrogen occupancy. To do that we will have to make some assumptions on the hydrogen interactions in the

metallic matrix. These assumptions are based on the experimental results outlined in Secs. II and III and can be summarized as follows. (1) Hydrogen occupies interstitial tetrahedral sites in the amorphous matrix. (2) Among these sites, those formed of four titanium atoms are preferentially occupied. (3) There exists some repulsive interaction between hydrogen atoms at small distance.

The procedure of analysis of the interstitial sites has already been presented in Sec. II. The result of the Voronoi decomposition of the structure into tetrahedra is shown in Fig. 13(a). For comparison, the statistical repartition of the same total number of sites (5.98 tetrahedral sites per metal atom) for a disordered alloy of atoms with the same size is also shown in Fig. 13(b). The number of $Ti_4$ sites increases from 0.37 per metal atom for the statistical distribution to 1.77 per metal atom in the microsegregated case, which is about twice the experimental hydrogen-to-metal ratio in amorphous CuTi hydrides at the equiatomic composition.[1,19–22]

The effective number of occupied sites will be now limited by the short-range hydrogen-hydrogen repulsive interaction. We make the assumption that this repulsive interaction prevents the simultaneous occupancy of face-sharing tetrahedra (nearest-neighbor sites). To do that, we use a procedure of simulated annealing in which one tries to maximize the total number of occupied sites while minimizing until zero the number of nearest-neighbor hydrogen atoms. Thus we do not consider any *a priori* exclusion distance, which seems to be more reasonable in the case of an amorphous alloy with a distribution of interatomic distances, leading to a continuous distribution of intersites distances extending almost down to zero. The resulting number of occupied sites is $n_H=0.74$ per metal atom, that is 42% of the initial number of $Ti_4$ sites. A simple random filling of sites with nearest-neighbor exclusion and without optimization leads to a much smaller hydrogen-to-metal ratio ($n_H=0.64$ per metal atom).

Such a value of 0.74 hydrogen per metal compares very well with the experimental results at this composition of $Cu_{50}Ti_{50}$, i.e., from 0.68 to 0.75 hydrogen per metal for pressure-charged samples[19,22] and from 0.70 to 0.84 hydrogen per metal for electrolytically charged samples.[1,20,21] The agreement appears to be systematically better for pressure-charged samples, which indicates that there are slightly more available sites in electrolytically charged samples, as a possible consequence of the different way of hydrogen loading. This can be related to the larger width of the small-angle maximum in Fig. 11, which also indicated that the sample was less "homogeneous" than the computer model, and maybe also than the pressure-charged sample.

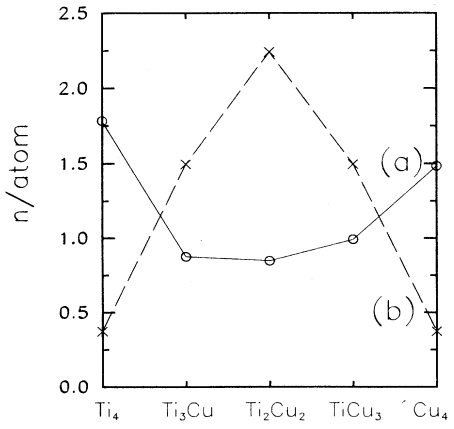


FIG. 13. Repartition of the $Cu_{4-n}Ti_n$ sites in the case of the microsegregated model (a) and comparison with the disordered model with no size effect (b).

Harris *et al.*[6] recently proposed a universal model for hydrogen absorption in amorphous transition metal alloys, on the basis of electrochemical measurements on Ni-Zr, Pd-Ti, and Ni-Ti alloys. They were able to fit their results with a model assuming a composition- and temperature-independent occupancy of interstitial sites $A_nB_{4-n}$ with a maximum hydrogen-to-metal ratio within each type of site given by

$$H/M=1.9\frac{4!}{n!(4-n)!}x^n(1-x)^{4-n},$$

$x$ being the Ti or Zr concentration. In such a model, the amorphous alloy is supposed to be chemically disordered and made of atoms of the same size, and the prefactor of 1.9 accounts for the blocking of nearest-neighbor sites. Harris *et al.* applied their model to the case of amorphous Cu-Ti hydrides and fitted the experimental variation of the hydrogen-to-metal ratio to the theoretical one. In this case, the hydrogen content of these amorphous Cu-Ti alloys would correspond to the occupation of $Ti_4$, $Ti_3Cu$, and a fraction (22%) of $Ti_2Cu_2$ sites whatever the alloy composition. The results we present here totally disagree with their model, since both experiment and simulation unambiguously show that the hydrogen-loaded samples are phase separated at a small scale, and thus very different from a chemically disordered alloy. Moreover, supposing that all the $Ti_4$ and $Ti_3Cu$ sites and 22% of the $Ti_2Cu_2$ sites were effectively occupied by hydrogen atoms, the relative contribution of the Ti-H and Cu-H nearest-neighbor distances in the total neutron atomic distribution function (taking into account the scattering lengths of titanium and copper) would be 55% for Ti-H and 45% (with an opposite sign) for Cu-H at the equiatomic composition, and 48% and 52% for the $Cu_{67}Ti_{33}$ alloy. One would, therefore, observe both contributions in the total $G(r)$, or no contribution at all if the Ti-H and Cu-H distances are not different enough from each other. This is clearly not the case according to our experimental results.[1,3]

To confirm this point, Fig. 14 presents the variation of the hydrogen-to-metal ratio in Cu-Ti amorphous alloys as a function of alloy composition. The different symbols are the experimental results, whereas the dotted line corresponds to the model of Harris *et al.*[6] The solid line corresponds to our simulation experiments. Starting from alloys of atoms of the same size but with different compositions (and thus neglecting size effect), we followed the same procedure as above (small-scale phase separation, occupancy of $Ti_4$ sites with nearest-neighbor

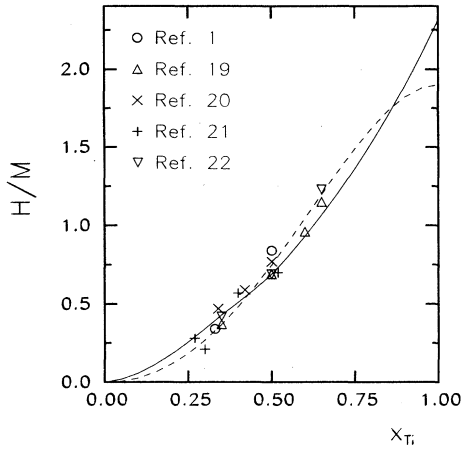


FIG. 14. Variation of the hydrogen-per-metal ratio with composition in Cu-Ti amorphous alloys: Model of Harris *et al* (Ref. 6) assuming a chemically disordered alloy and the occupancy of $Ti_4$, $Ti_3Cu$, and 22% of $Ti_2Cu_2$ sites (dotted line), our results assuming a microsegregated alloy and occupancy of $Ti_4$ sites only (solid line), experimental results (symbols).

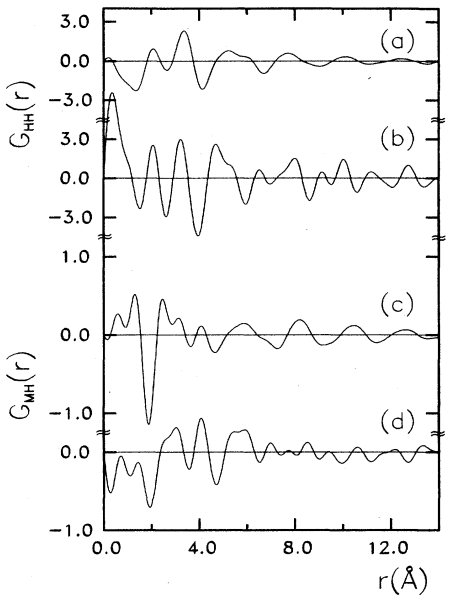


FIG. 15. Simulated (top curve) and experimental (bottom curve) partial hydrogen-hydrogen (a) and (b) and metal-hydrogen (c) and (d) reduced atomic distribution functions.

exclusion) to determine the maximum hydrogen content as a function of alloy composition. From Fig. 14 it appears that our simulation gives as good an agreement with experimental hydrogen content as the model of Harris *et al.* with the additional advantage that it also agrees with the neutron-diffraction results.

Our computer calculations give us both the structure of the metallic CuTi matrix and the location and number of hydrogen atoms (which are set at the center of their tetrahedral sites). Therefore it is now possible to compare experimental and simulated partial $G(r)$ and $S(q)$ curves for the hydrogen-hydrogen and metal-hydrogen correlations, as we did above for the partial metal-metal ones [cf. Eqs. (4) and (5)]. But in this case one has to extract these partial functions from three experiments with different hydrogen-deuterium ratio. Let us just recall that, although the system to be solved is quite well conditioned because of the large amplitude of possible variation of the scattering length of the hydrogen-deuterium mixture (from $-0.374\times10^{-12}$ cm for hydrogen to $+0.667\times10^{-12}$ cm for deuterium), the difficulty for correcting neutron-scattering curves of hydrogenated amorphous alloys will introduce even larger experimental errors for the extraction of partial functions than in the case of the determination of total functions. The comparison with the simulated partial functions will thus be only qualitative.

Figure 15 compares experimental and simulated partial hydrogen-hydrogen and metal-hydrogen reduced atomic distribution functions $G_{HH}(r)$ and $G_{MH}(r)$. On both experimental and simulated $S(q)$ curves (not shown), the small-angle maximum has not been taken into account in the Fourier transform (by introducing a small-$q$ cutoff). Such a procedure was used because one of the three experimental $S(q)$ (that corresponding to the hydrogenated sample) was recorded on a smaller $q$ range than the two other ones, preventing from the observation of the small-angle maximum. Although the poor definition of the $S_{HH}(q)$ and $S_{MH}(q)$ functions introduces parasitic oscillations in the Fourier transforms, two main peaks can be observed on $G_{HH}(r)$ at about 2.0 and 3.2 Å, which are almost independent of the cutoff distance in reciprocal space. This is not the case of peaks appearing at distances smaller than 2 Å, which have thus no physical meaning. One can see that these peaks closely correspond to those observed on the simulated curve. Thus the comparison between simulated and experimental functions seems to support the assumption of the existence of a short-range hydrogen-hydrogen repulsive interaction in these amorphous alloys, as in the case of crystalline hydrides. A qualitative agreement is also obtained for the $G_{MH}(r)$ curves. Except for the first negative peak at 1.9 Å corresponding to the Ti-H nearest-neighbor distance, it is difficult to identify the other peaks at larger distance since this partial function is the weighted sum of the Cu-H and Ti-H partial reduced atomic distribution functions with positive and negative contributions, respectively [cf. Eq. (5)].

Finally Fig. 16 presents the total atomic distribution functions $G(r)$ corresponding to the hydrogenated and deuterated samples, along with the simulated curves. The differences observed between experimental and simulated partial functions are obviously reproduced in the total functions. Nevertheless a satisfactory agreement is obtained for distances smaller than about 8 Å.

Another test of our computer model is to study the variation of the intensity of the small-angle maximum with the hydrogen-deuterium substitution. In paper I we presented the experimental variation of this intensity for three samples with different hydrogen-deuterium ratio.

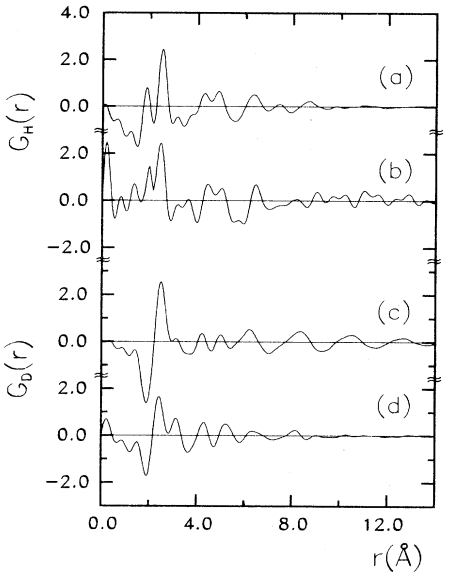


FIG. 16. Total simulated (top curve) and experimental (bottom curve) reduced atomic distribution functions $G(r)$ for the hydrogenated (a) and (b) and deuterated (c) and (d) alloys.

In the framework of a two-phase model, we were able to estimate the composition of the two phases, keeping in mind that such a model was only a crude approximation of the actual situation since, for such a small-scale phase separation, the transition region between copper-rich and titanium-hydrogen-rich phases was certainly not negligible. Since the scattered intensity per atom $I_a(q)$ is related to the interference function $S(q)$ through $I_a(q) = \langle b^2 \rangle S(q)$, it follows from Eq. (2) that

$$I_a(q) = \langle b^2 \rangle + \sum_i \sum_j c_i c_j b_i b_j [S_{ij}(q) - 1] , \qquad (6)$$

where the $S_{ij}(q)$ are the partial interference functions. Considering a ternary Cu-Ti-H alloy, Eq. (6) is thus a quadratic function of the three scattering lengths $b_i$. The three experimental curves can be used to calculate the value of $b_{H,D}$ at which the small-angle intensity will be minimum (but not zero contrary to the case of the two-phase model). This minimum is found for $b_{H,D} = +0.66 \times 10^{-12}$ cm. Turning now to the simulation results, the variation of $I_a(q)$ versus $b_{H,D}$ is directly obtained from Eq. (6) since the six partial functions $S_{ij}(q)$ are calculated from the six corresponding $G_{ij}(r)$ functions. In this case the minimum of $I_a(q)$ is found at $b_{H,D} = +0.63 \times 10^{-12}$ cm, very close to the experimental value.

## VI. DISCUSSION

On the basis of the results presented in this paper, it appears that there are at least three essential parameters to be considered if one wants to study the hydrogen-absorption properties of transition-metal amorphous alloys, which are the degree of chemical order in the alloy, the type of interstitial sites to be occupied by the hydrogen atoms, and the short-range interaction between hydrogen atoms. In addition, the size difference between atoms is a less important but non-negligible parameter. These parameters are important since almost all the amorphous alloys of this type studied up to now are not chemically disordered and exhibit more or less size effect. On the other hand, the chemical nature of sites for hydrogen absorption is not clearly established in most cases, and the existence of a short-range hydrogen-hydrogen repulsive interaction has never been experimentally observed.

In principle neutron-diffraction experiments would be able to answer all these questions since isotopic substitution on both metal atoms and hydrogen atoms can lead to the determination of the six metal-metal, metal-hydrogen, and hydrogen-hydrogen partial pair correlation functions in the case of a ternary hydride. From that, one can directly measure the degree of chemical ordering of the metallic matrix, the metal-hydrogen coordinances (and thus the chemical nature of the hydrogenation sites), and the hydrogen-hydrogen nearest-neighbor distances.

That is what we tried to do to some extent in the case of amorphous CuTi hydrides, the hydrogen-deuterium substitution allowing us to determine three partial metal-metal, metal-hydrogen, and hydrogen-hydrogen correlation functions. Unfortunately the potential accuracy of such a substitution (resulting from the good contrast between hydrogen and deuterium) is counter balanced by two problems. The first one is the difficulty of correcting neutron-scattering curves of hydrogen-containing alloys. The second one is related to the amorphous CuTi alloy itself. Since hydrogen greatly changes the structure of the matrix, it is thus difficult to be sure that the unique effect of the hydrogen-deuterium substitution is to change the scattering length of the hydrogen atoms, without any other change of the matrix. This is a general problem of the isotopic substitution in which one has to work with different samples, contrary to the case of anomalous x-ray diffraction, for example, where a unique sample is used (but with a smaller amplitude of variation of the scattering factors). This problem is amplified in the case of our CuTi alloys by comparison to other hydrides in which hydrogen occupies only interstitial sites without modification of the amorphous matrix (Except for a dilation of the metal-metal distances upon hydrogen absorption). Nevertheless our neutron-diffraction experiments have unambiguously shown that (i) the initially chemically ordered CuTi alloy changes to a microsegregated one upon hydrogen absorption, (ii) there are preferential Ti-H nearest-neighbor correlations, and (iii) there exists some repulsive short-range interaction between hydrogen atoms.

Based on these experimental informations, the computer models presented here well reproduced both the structure of the metallic matrix before and after hydrogen loading and the location of the hydrogen atoms in the microsegregated alloy. The obtained maximum hydrogen content is also in agreement with the experimental results, whatever the alloy composition. These calculations confirm that the knowledge of the degree of chemical order is essential for the study of the hydrogen-absorption

properties of amorphous alloys. This is quite evident in the CuTi system where hydrogen leads to a transformation of the amorphous matrix. This is also true in other systems where diffraction experiments indicate the presence of chemical ordering.

The numerical methods presented here (Monte Carlo procedure with nearest-neighbor exchanges and relaxation method) were used in order to obtain both starting ordered and final phase-separated states similar to the experimental ones. We did not try to vary the interatomic distances, depths of the potentials or degree of order in a systematic way for the different models considered in order to obtain the best possible agreement with the experimental data. In the same way, we decoupled ordering and relaxation procedures for the sake of simplicity, whereas both processes simultaneously occur in the real CuTi alloy. Finally, the hydrogen atoms were introduced in a "rigid" CuTi matrix, by filling only the tetrahedral $Ti_4$ sites with H-H nearest-neighbor exclusion, and thus ignoring any possible relaxation of the hydrogen-hydrogen interactions. Such effects could be taken into account to some extent by a numerical relaxation of the ternary alloy, but would require a knowledge of the hydrogen-metal and hydrogen-hydrogen interaction potentials.

Concerning the physical mechanism of the transformation of the matrix upon hydrogen absorption, one could imagine that, as the hydrogen concentration increases, the hydrogen atoms first occupy the $Ti_4$ sites in the chemically ordered matrix (up to about 0.15 hydrogen per metal), until no available site is left. This would be in agreement with our first neutron-diffraction experiments on samples with smaller hydrogen contents[3] which showed that the main effect of hydrogen on the pair correlation function was the appearance of Ti-H correlations, without any large modification of the rest of the curve. Beyond that "critical" hydrogen concentration, microphase separation would then result in the progressive creation of new $Ti_4$ sites, up to a hydrogen-to-metal ratio of about 0.70 to 0.80 at which the whole matrix would be transformed.

[1]B. Rodmacq, M. Maret, J. Laugier, L. Billard, and A. Chamberod, Phys. Rev. B **38**, 1105 (1988).
[2]B. Rodmacq and A. Chamberod, Phys. Rev. B **38**, 1116 (1988).
[3]B. Rodmacq, Ph. Mangin, and A. Chamberod, J. Phys. F **15**, 2259 (1985).
[4]H. Kaneko, T. Kajitani, M. Hirabayashi, M. Ueno, and K. Suzuki, J. Less-Common Met. **89**, 237 (1983).
[5]K. Samwer and W. L. Johnson, Phys. Rev. B **28**, 2907 (1983).
[6]J. H. Harris, W. A. Curtin, and M. A. Tenhover, Phys. Rev. B **36**, 5784 (1987).
[7]A. C. Switendick, Z. Phys. Chem. **117**, 89 (1979); K. H. J. Buschow, P. C. Bouten, and A. R. Miedema, Rep. Prog. Phys. **45**, 937 (1982).
[8]E. Batalla, J. O. Strom-Olsen, Z. Altounian, D. Boothroyd, and R. Harris, J. Mater. Res. **1**, 765 (1986).
[9]F. Lançon, Ph.D. Thesis, University Grenoble, 1984.
[10]F. Lançon, L. Billard, and A. Chamberod, J. Phys. F **14**, 579 (1984).
[11]T. E. Faber and J. M. Ziman, Philos. Mag. **11**, 153 (1965).
[12]F. Spaepen and G. S. Cargill, III, in *Proceedings of the 5th International Conference on Rapidly Quenched Metals,* edited by S. Steeb and H. Warlimont (North-Holland, Amsterdam, 1985), p. 581; G. S. Cargill, III and F. Spaepen, J. Non-Cryst. Solids **43**, 91 (1981).
[13]A. B. Bhatia and D. E. Thornton, Phys. Rev. B **2**, 3004 (1970).
[14]C. N. J. Wagner and H. Ruppersberg, At. Energy Rev. **1**, 101 (1981).
[15]K. Kawasaki, in *Phase Transition and Critical Phenomena,* edited by C. Domb and M. S. Green (Academic, New York, 1972), Vol. 2, p. 443.
[16]B. J. Gellatly and J. L. Finney, J. Non-Cryst. Solids **50**, 313 (1982).
[17]M. Sakata, N. Cowlam, and H. A. Davies, J. Phys. (Paris) Colloq. **41**, C8-190 (1980).
[18]B. Rodmacq, L. Billard, Ph. Mangin, and A. Chamberod, J. Phys. (Paris) Colloq. **46**, C8-415 (1985).
[19]A. J. Maeland, L. E. Tanner, and G. G. Libowitz, J. Less-Common Met. **74**, 279 (1980).
[20]B. Grzeta, K. Dini, N. Cowlam, and H. A. Davies, J. Phys. F **15**, 2069 (1985).
[21]Y. S. Lee and D. A. Stevenson, J. Non-Cryst. Solids **72**, 249 (1985).
[22]C. H. Hwang, S. Kang, K. Cho, and K. Kawamura, Scr. Metall. **20**, 1231 (1986).